Voluminous plutonism during a period of volcanic quiescence revealed by thermochemical modeling of zircon

Casey R. Tierney[1,2], Axel K. Schmitt[3,4], Oscar M. Lovera[3] and Shanaka L. de Silva[1]

[1] College of Earth, Ocean, and Atmospheric Sciences, Oregon State University, Corvallis OR 97331, USA

[2] School of Earth Sciences and Environmental Sustainability, Northern Arizona University, 625 S Knoles Dr, Flagstaff AZ 86011, USA

[3] Department of Earth, Planetary, and Space Sciences, University of California, Los Angeles CA 90095, USA

[4] Institut für Geowissenschaften, Universität Heidelberg, Im Neuenheimer Feld 234-236, 69120 Heidelberg

SUPPLEMENTAL INFORMATION

Analytical Methods

Rock samples for $^{40}Ar/^{39}Ar$ geochronology (Supplementary Table 1) were dated at the Rare Gas Geochronology Lab at the University of Wisconsin, Madison where biotite was separated by first crushing the rock then picking euhedral biotite crystals. Biotite crystals were then cleaned ultrasonically in dilute (5%) nitric acid for one minute to remove any glass. Once separated the sanidine and biotite crystals were placed in Al foil packets which were then placed in into wells in Al disks interspersed with 28.34 Ma sanidine standard from the Taylor Creek rhyolite (Renne et al., 1998). The Al disks were then loaded and irradiated for three hours in the TRIGA research reactor at Oregon State University. Once irradiated the crystal samples were returned to

University of Wisconsin where biotite was analyzed via Single-Crystal laser-fusion (SCLF). During this process, biotite was treated with a 0.1 Watt clean-up using a defocused laser beam to release loosely bound, atmospherically absorbed, argon. Following this clean-up, the biotite was fused for 75 s and then followed by gas clean-up on two SAES GP50 getters for 600 s. Isotopic analysis and data reduction followed the procedures of Smith et al. (2003).

Zircon U-Th, U-Pb, and trace element analyses by CAMECA ims 1270 SIMS (Supplementary Table 2) at the University of California Los Angeles followed established protocols (Reid et al., 1997) modified according to Schmitt (2011). Multi-collection U-Th analyses are considered accurate to within ~2% based on replicate analyses of secular equilibrium reference zircon AS3 which yielded $(^{230}Th)/(^{238}U) = 1.021 \pm 0.006$ (MSWD = 1.3; n = 34) in analyses interspersed with the unknowns. $^{206}Pb/^{238}U$ dating followed procedures in Schmitt et al. (2003). Reference zircon $^{206}Pb/^{238}U$ ages have an external reproducibility of 2.3% (1 standard deviation for the AS3 age; n = 49) and are accurate to within 0.85% based on a comparison with reference zircon 91500 (n = 2). Zircon trace element uncertainties are estimated from replicate analyses of reference zircon 91500 (n = 5). Standard zircon details and references are available in Supplementary Table 2. Representative trace elements Ti, Gd, Yb, and Hf are reproducible to within 8.6%, 4.8%, 3.3%, and 1.5% (1 standard deviation) and negligibly (by +11%, -3.4%, +3.2%, and -2.5%, respectively) deviate from reference values (Supplementary Table 2).

Thermochemical Modeling

A 2-D thermal diffusion model with temperature dependent diffusivity-conductivity and incorporating the effects of magma recharge, assimilation, and fractional crystallization (RAFC) was developed using a finite difference discretization by the alternating-direction implicit

method (Press et al., 1998). All calculations were run on a grid of 20 × 60 km (wide × depth), and cell sizes of 0.1×0.1 km.

The heat diffusion equation is solved for temperature dependent diffusivity-conductivity ($\kappa(T)$,$C_p(T)$) following the equations in Whittington et al., (2009):

$$\kappa(mm^2 s^{-1}) = \begin{cases} 567.3/T - 0.062 \quad ; & T \le 846K \\ 0.732 - 0.000135T \quad ; & T > 846K \end{cases} \tag{1a}$$

$$C_p(J\,mol^{-1}K^{-1}) = \begin{cases} 199.50 + 0.0857T - 5.0\times10^6\,T^{-2} & T \le 846K \\ 229.32 + 0.0323T - 47.9\times10^{-6}\,T^{-2} & T > 846K \end{cases} \tag{1b}$$

(κ = thermal diffusivity; C_p = heat capacity at constant pressure).

Crustal assimilation (only of limited importance in these models because of the comparatively shallow emplacement with cold wall rocks) uses the parameterization of Spera and Bohrson, (2001). The following parameters were used in the model:

Fractional Crystallization (T_{lq} = magma liquidus temperature; T_s = magma solidus temperature):

$$X = (T_{lq} - T)/(T_{lq} - T_s) \tag{2a}$$

$$F_m = 1 - X^2 \qquad T_s \le T \le T_{lq} \tag{2b}$$

$$if\ T < T_s \Rightarrow F_m = 0;\ if\ T > T_{lq} \Rightarrow F_m = 1 \tag{2c}$$

Assimilation (F_c = fraction of melted and assimilated country rock):

$$X = (T - T_s)/(T_{la} - T_s) \qquad T_s \le T \le T_{la};\ \ a = 0.005 \tag{3a}$$

$$F_c = \begin{cases} a \times (e^{2\times\ln(100)\times X} - 1) & X \le 0.5 \\ 1 - a * e^{2\times\ln(100)\times(1-X)} & X > 0.5 \end{cases} \quad (3b)$$

$$if\ T < T_s \Rightarrow F_c = 0;\ if\ T > T_{la} \Rightarrow F_c = 1 \quad (3c)$$

Sensitivity tests agree well with published conductive cooling models (Gelman et al., 2013; Caricchi et al., 2014). Initial recharge magma temperature was 1000 °C in agreement with thermometry for mafic lavas in the Chascon-Runtu Jarita complex (Watts et al., 1999). An initial geothermal gradient of ~50 °C/km was imposed as the background thermal state of the instantaneous ellipsoidal magma intrusion of ~50 km^3 emplaced at the <10 km depth consistent with the thermobarometry of the APVC domes. Note that even when a constant heat flux is imposed at the 20 km bottom of the grid, the temperature (~1000°C) agrees well with the magma recharge temperature and the estimated top of the hot zone temperature (Chmielowski et al., 1999).

In contrast to previous models (Caricchi et al., 2014), zircon generated in each cell was quantified taking into account the thermal and compositional dependence of zircon saturation (Boehnke et al., 2013). This model is unique in that it calculates the relative abundance of zircon F_{zrc} as a function of temperature. An experimentally calibrated relation between zircon saturation, temperature, and melt compositions was presented in Harrison et al. (2007) for magmas with intermediate compositions. Harrison et al. (2007) used experimental glass compositions from Carroll and Wyllie (1989;1990) to determine the compositional parameter M (= [Na+K+2×Ca]/Al×Si; Boehnke et al. 2013) as a function of T. Zircon saturation was then

calculated as a function of M and T by applying the recent re-calibration for zircon saturation in Boehnke et al. (2013) leading to the parameterization:

$$F_{zrc}\,(\%) = 162 - 1.8\times10^{-6} e^{-10^4/T};\ T_s \geq T \leq T_{zsat}\ if\ T < T_s \Rightarrow F_{zrc} = 1;\ if\ \ T > T_{zsat} \Rightarrow F_{z\,rc} = 0 \qquad (4)$$

No significant differences in modeled recharge rates required to match the observed zircon age spectra were observed for modeling zircon saturation with the original Watson and Harrison (1983) calibration. This attests to the robustness of the zircon saturation model. Because zircon rim ages represent only a fraction of the mass of individual zircons (a rim analysis with ~5 µm crater depth represents ~30% of the mass, for a spherical crystal with 50 µm radius) the model sums only the last 30% of zircon crystallized in each cell, weighted by the total fraction of zircon crystallized at the time of eruption. The average age of the last 30% of zircon crystallized is then calculated, corresponding to the ~30% volume percentage of zircon sampled by depth profile analysis.

Periodic instantaneous episodes of recharge at the center of the chamber are simulated, followed by radial outward growth of the magma chamber following the mass conservation law. A more protracted built-up extends the duration of zircon crystallization, but does not significantly alter the relative abundances of newly formed vs. recycled zircons. Similarly, changing intrusion geometry or timing (in the current model every 5 ka) yields qualitatively similar zircon crystallization patterns.

Supplementary Figures

Supplementary Fig. 1: U from trace element analysis vs. U from geochronologic analysis. Trace element analyses targeted the same craters as for geochronology. The scatter in U abundances is due to small-scale heterogeneities in the U abundances of zircon, but the data plot near the 1 : 1 line ensuring comparability between both data sets.

Supplementary Fig. 2: Measured rare earth element (REE) abundances in zircon (a, c, e, g, i) and whole rocks (b, d, f, h, j). The whole rock plot also compares the actual abundances with those modeled for the melt using published zircon-melt distribution coefficients (Sano et al., 2002). With the exception of La (a difficult to measure light REE for which D values might be poorly constrained), zircon-based REE abundances agree with those analyzed in whole rocks, indicating that zircon crystallized from melts similar to those represented by whole rock compositions.

Supplementary Fig. 3: Zr/Hf vs. Ti in zircon. Ti in zircon is directly temperature (T) dependent (Ti-in-zircon)[12] and correlates well with Zr/Hf, an indirectly T-dependent compositional parameter (Claiborne et al., 2010). This supports Ti-in-zircon variations to indicate the thermal evolution of the magma.

Supplementary Fig. 4: Activity $aTiO_2$ vs. T for zircon and Fe-Ti oxides. **a** One dimensional probability distribution for fixed $a\mathrm{TiO_2} = 0.8$. **b** Two-dimensional probability distribution of T_{Tiz} with variable $a\mathrm{TiO_2}$. Isopleths were calculated using the calibration from Ferry and Watson (2007) assuming melt $a\mathrm{SiO_2} = 1$. Individual analyses and uncertainties are color coded according to their probability. Colored circles show $a\mathrm{TiO_2}$ and temperature T calculated for Fe–Ti oxides in domes using the calibration of Ghiorso and Gualda (2012).

Supplementary Fig. 5: Ti vs. age for zircons from APVC domes. Ti-in-Zircon temperatures determined are shown in scales to right of each dome for both 0.7 and 0.9 $a\mathrm{TiO_2}$. Dashed lines show cooling rate of 10^{-4} °C/a for both 0.7 and 0.9 $a\mathrm{TiO_2}$. Temperatures determined from Ferry and Watson (2007) using $a\mathrm{TiO_2}$ values determined in Supp. Fig. 4. Gray bar in panel e represents Ar-Ar sanidine eruption age (Dunne, 1998).

Supplementary Fig. 6: Temperature dependence of zircon fraction (F_{zrc}), fraction of remaining melt (F_m), and fraction of assimilated country rock (F_c) used in thermochemical model calculations. F_m and F_{zrc} curves are based on Harrison et al. (2007) modified by using the more recent calibration for zircon saturation from Boehnke et al. (2013). F_c is based on a typical temperature-assimilation relationship in Spera and Bohrson (2001). We note that because of the comparatively low T of the shallow country rock, assimilation is negligible, consistent with the scarcity of xenocrystic zircon in the APVC lavas.

Supplementary Fig. 7: Example recharge-assimilation-fractional crystallization (RAFC) 2-D model cross section for 60 km width × 20 km depth and 0.1 × 0.1 km^2 cell resolution. Finite difference discretization is carried out using the alternating-direction implicit method. Red area shows extent of initially emplaced ~50 km^3 ellipsoid pluton, purple spot represents instantaneous emplacement of magma in the center of the original magma chamber, and gray ellipsoid the expansion of the magma body following recharge. The crust has a fixed steady-state geotherm (50 °C/km; 25 °C at the surface; 1,000 °C at 20 km depth) which reflects the presence of the Altiplano Puna Magma Body (APMB) and the thermal priming of the crust during the flare up (de Silva and Gosnold, 2007).

Supplementary Fig. 8: Recharge-assimilation-fractional crystallization (RAFC) 2-D model cross sections at 8 representative time slices. Hatched area shows extent of initially emplaced ~50 km^3 ellipsoid pluton, black line indicates extent of batholithic crust. Time-slices (a-h) are selected to represent the thermal evolution of a shallow intrusion via recharge with the emplacement of the initial magma at t = 600 ka (which corresponds to ca. 500 ka prior to eruption of the APVC domes). Periodical episodes of recharge are modeled as instantaneous emplacement of magma in the center of the original magma chamber (every 5 ka at a time-integrated rate of 1.08×10^{-3} km^3/a), which in this case terminates at 500 ka. See Supplementary Figure 7 for additional model details.

Supplementary Tables

Supplementary Table 1: Biotite $^{40}Ar/^{39}Ar$ ages. $^{40}Ar/^{39}Ar$ eruption ages were obtained for each dome (sanidine for Chascon-Runtu Jarita (Dunne, 1998); biotite for the other four domes) and range between ca. 87 and 120 ka. Biotite ages define the upper limit of this range, and are considered maximum ages due to the likely presence of unsupported ^{40}Ar (Hora et al., 2010). We therefore interpret the eruption age of all these domes to be ~85–100 ka. This is consistent with the youngest dates revealed by zircon rims from each dome.

Supplementary Table 2: Zircon geochronology and trace element data. Details related to reference zircons AS3 and 91500 are located in Paces and Miller (1993) and Wiedenbeck et al. (1995), respectively.

Supplementary Table 3: Summary of Thermal Model Parameters.

References Cited

Boehnke, P., Watson, E.B., Trail, D., Harrison, T.M., and Schmitt, A.K., 2013, Zircon saturation re-revisited: Chemical Geology, v. 351, p. 324–334

Caricchi, L., Simpson, G., and Schaltegger, U., 2014, Zircons reveal magma fluxes in the Earth's crust: Nature, v. 511, p. 457–461

Carroll, M. R., and Wyllie, P. J., 1989, Experimental phase relations in the system tonalite-peridotite-H_2O at 15 kb; implications for assimilation and differentiation processes near the crust-mantle boundary: Journal of Petrology, v. 30(6), p. 1351-1382.

Carroll, M. R., and Wyllie, P. J., 1990, The system tonalite-H_2O at 15 kbar and the genesis of calc-alkaline magmas: American Mineralogist, v. 75, p. 345–357.

Chmielowski, J., Zandt, G., and Haberland, C., 1999, The Central Andean Altiplano-Puna Magma Body: Geophysical Research Letters, v. 26, p. 783–786.

Claiborne, L.L., Miller, C.F., Flanagan, D.M., Clynne, M.A., and Wooden, J.L., 2010, Zircon reveals protracted magma storage and recycling beneath Mount St. Helens: Geology, v. 38, p. 1011–1014.

de Silva, S. L., & Gosnold, W. D. (2007). Episodic construction of batholiths: Insights from the spatiotemporal development of an ignimbrite flare-up. Journal of Volcanology and Geothermal Research, v.167, p. 320–335.

Dunne, J.A., 1998, Calibration of the method of exposure dating of geomorphic surfaces on the earth using in-situ produced cosmogenic radionuclides, and applications in the Central Andes [PhD Thesis]: Purdue University, Indiana, 250 p.

Ferry, J.M., and Watson, E.B., 2007, New thermodynamic models and revised calibrations for the Ti-in-zircon and Zr-in-rutile thermometers: Contributions to Mineralogy and Petrology, v. 154, p. 429–437

Gelman, S.E., Gutierrez, F.J., and Bachmann, O., 2013, On the longevity of large upper crustal silicic magma reservoirs: Geology, v. 41, p. 759–762

Harrison, T.M., Watson, E.B., and Aikman, A.B., 2007, Temperature spectra of zircon crystallization in plutonic rocks: Geology, v. 35, p. 635–638.

Hora, J.M., Singer, B.S., Jicha, B.R., Beard, B.L., Johnson, C.M., de Silva, S., and Salisbury, M., 2010, Volcanic biotite-sanidine 40Ar/39Ar age discordances reflect Ar partitioning and pre-eruption closure in biotite: Geology, v. 38, p. 923–926.

Paces, J.B., and Miller, J.D., 1993, Precise U-Pb ages of Duluth Complex and related mafic intrusions, northeastern Minnesota: Geochronological insights to physical, petrogenetic, paleomagnetic, and tectonomagmatic processes associated with the 1.1 Ga Midcontinent rift System: Journal of Geophysical Research, v. 98, p. 13997–14013.

Press, W.H., Flannery, B.P., Teukolsky, S.A., and Vetterling, W.T., 1988, Numerical recipes: The art of scientific computing: Cambridge, Cambridge University Press.

Reid, M.R., Coath, C.D., Harrison, T.M., and McKeegan, K.D., 1997, Prolonged residence times for the youngest rhyolites associated with Long Valley Caldera: Th-238U ion microprobe dating of young zircons: Earth and Planetary Science Letters, v. 150, p. 27–39.

Renne, P.R., Swisher, C.C., Deino, A.L., Karner, D.B., Owens, T.L., and DePaolo, D.J., 1998, Intercalibration of standards, absolute ages and uncertainties in 40Ar/39Ar dating: Chemical Geology, v. 145, p. 117–152.

Sano, Y., Terada, K., and Fukuoka, T., 2002, High mass resolution ion microprobe analysis of rare earth elements in silicate glass, apatite and zircon: lack of matrix dependency: Chemical Geology, v. 184, p. 217–230.

Schmitt, A.K., 2011, Uranium Series Accessory Crystal Dating of Magmatic Processes: Annual Review of Earth and Planetary Sciences, v. 39, p. 321–349.

Schmitt, A.K., Grove, M., Harrison, T.M., Lovera, O., Hulen, J., and Walters, M., 2003, The Geysers - Cobb Mountain Magma System, California (Part 1): U-Pb zircon ages of volcanic rocks, conditions of zircon crystallization and magma residence times: Geochimica et Cosmochimica Acta, v. 67, p. 3423–3442

Smith, M.E., Singer, B., and Carroll, A., 2003, 40Ar/39Ar geochronology of the Eocene Green River Formation, Wyoming: Geological Society of America Bulletin, v. 115, p. 549–565.

Spera, F.J., and Bohrson, W.A., 2001, Energy-Constrained Open-System Magmatic Processes I: General Model and Energy-Constrained Assimilation and Fractional Crystallization (EC-AFC) Formulation: Journal of Petrology, v. 42, p. 999–1018.

Watson, E. B., and Harrison, T. M., 1983, Zircon saturation revisited: temperature and composition effects in a variety of crustal magma types. Earth and Planetary Science: Letters, v. 64(2), p. 295-304.

Watts, R.B., de Silva, S.L., de Rios, G.J., and Croudace, I., 1999, Effusive eruption of viscous silicic magma triggered and driven by recharge: a case study of the Cerro Chascon-Runtu Jarita Dome Complex in Southwest Bolivia: Bulletin of volcanology, v. 61, p. 241–264.

Whittington, A.G., Hofmeister, A.M., and Nabelek, P.I., 2009, Temperature-dependent thermal diffusivity of the Earth's crust and implications for magmatism: Nature, v. 458, p. 319–321

Wiedenbeck, M., Alle, P., Corfu, F., Griffin, W.L., Meier, M., Oberli, F., Von Quadt, A., Roddick, J.C., and Spiegel, W., 1995, Three natural zircon standards for U-Th-Pb, Lu-Hf, trace element and REE analyses: Geostandards Newsletter, v. 91, p. 1–23.

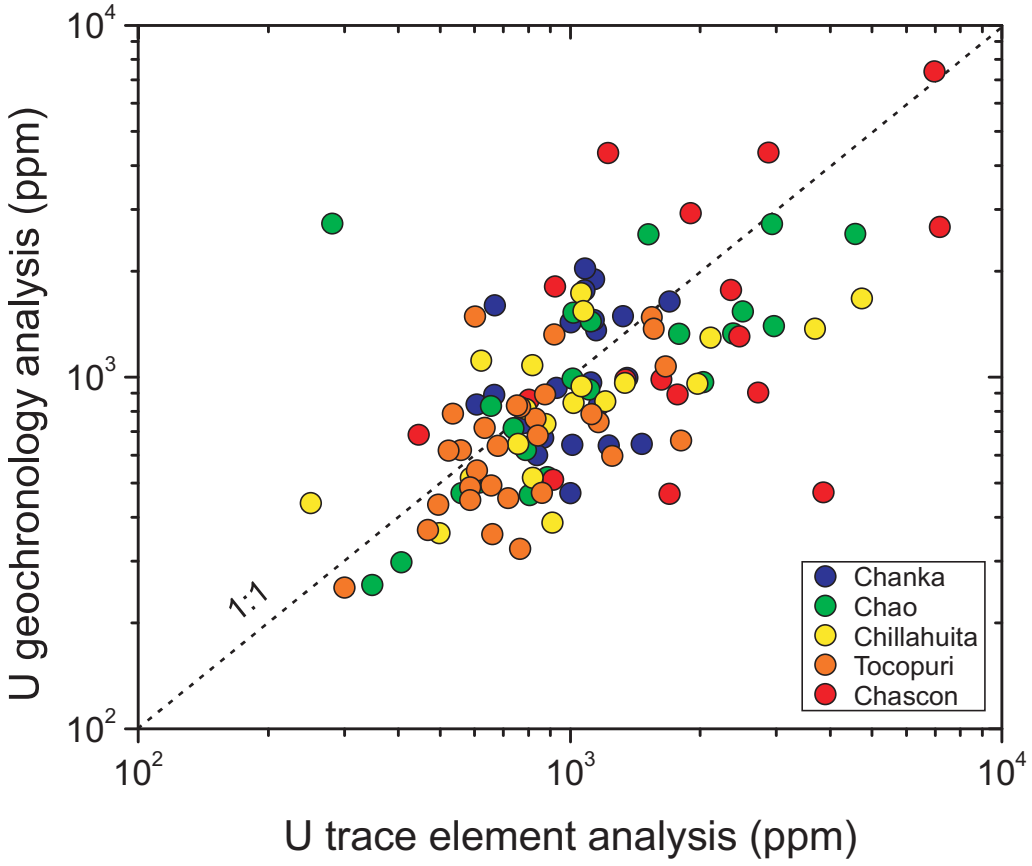

Tierney et al. Supplementary Figure 1

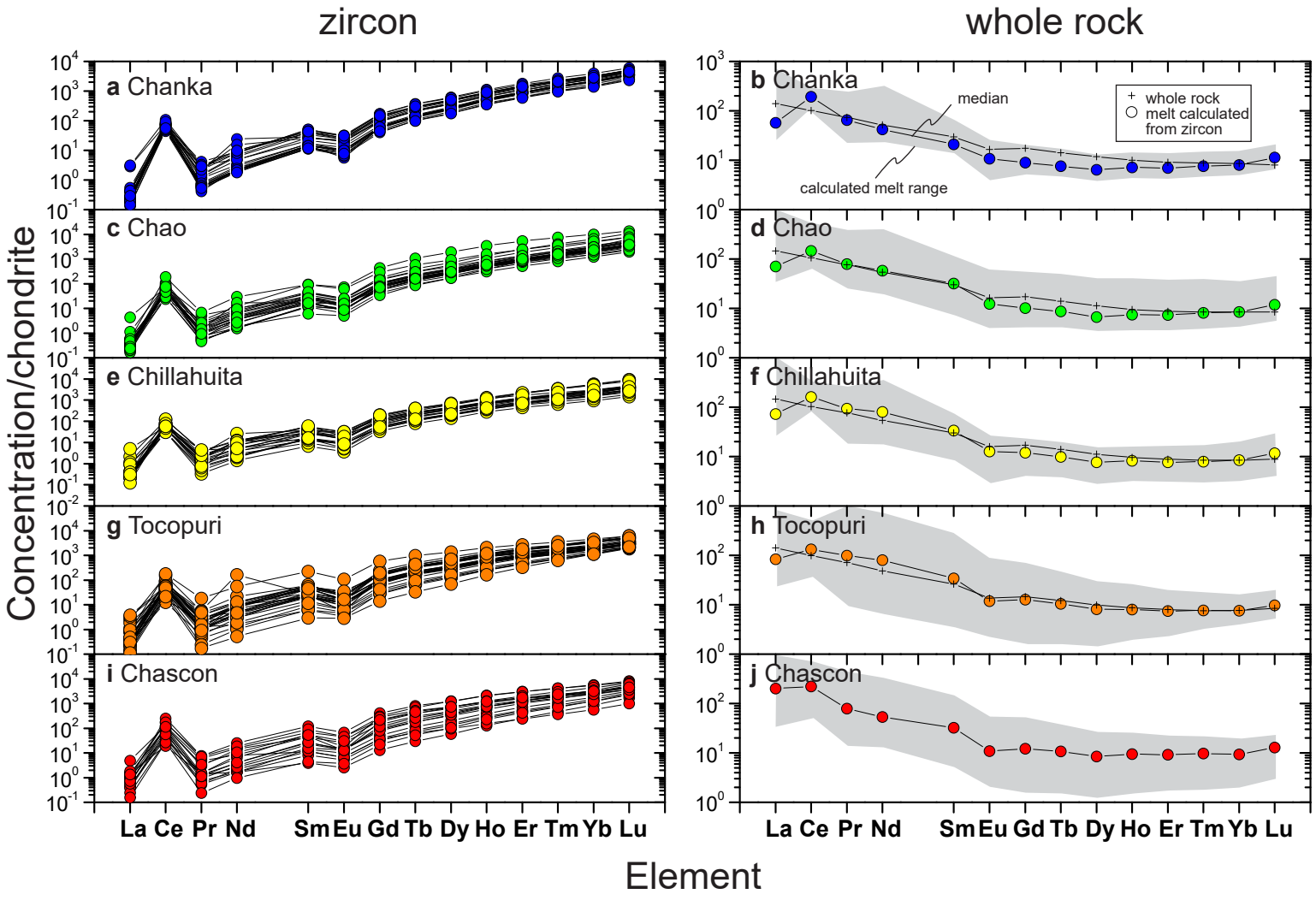

Tierney et al. Supplementary Figure 2

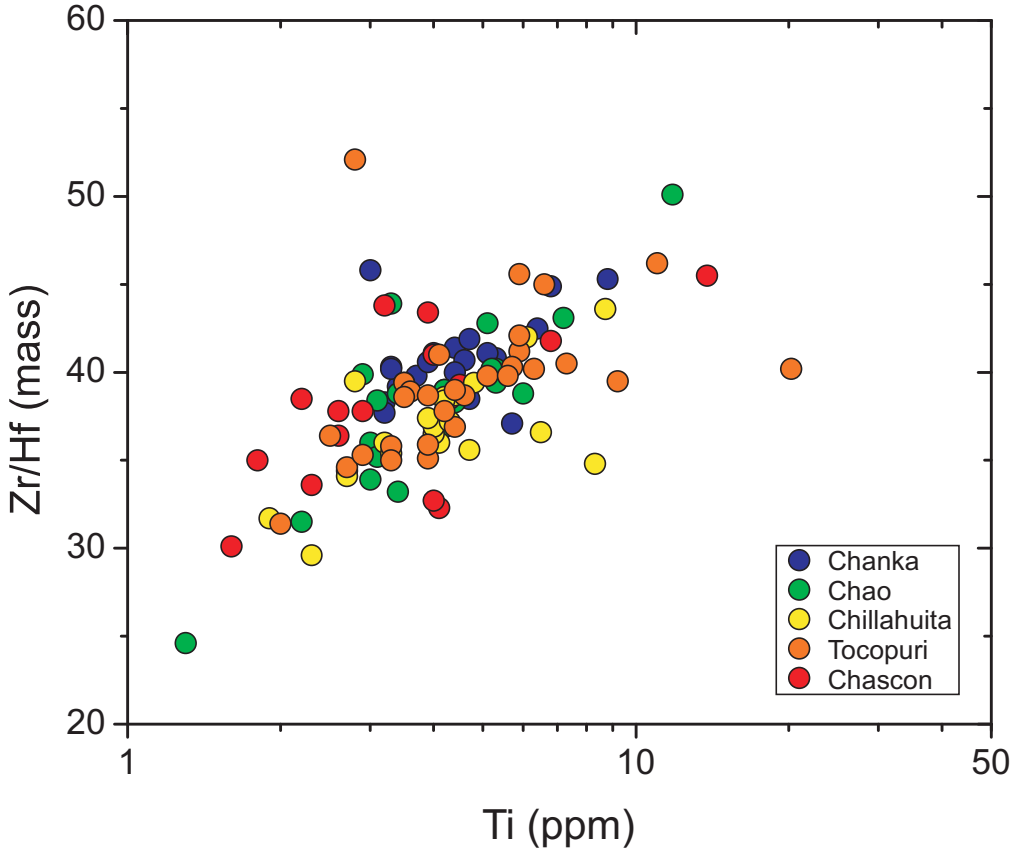

Tierney et al. Supplementary Figure 3

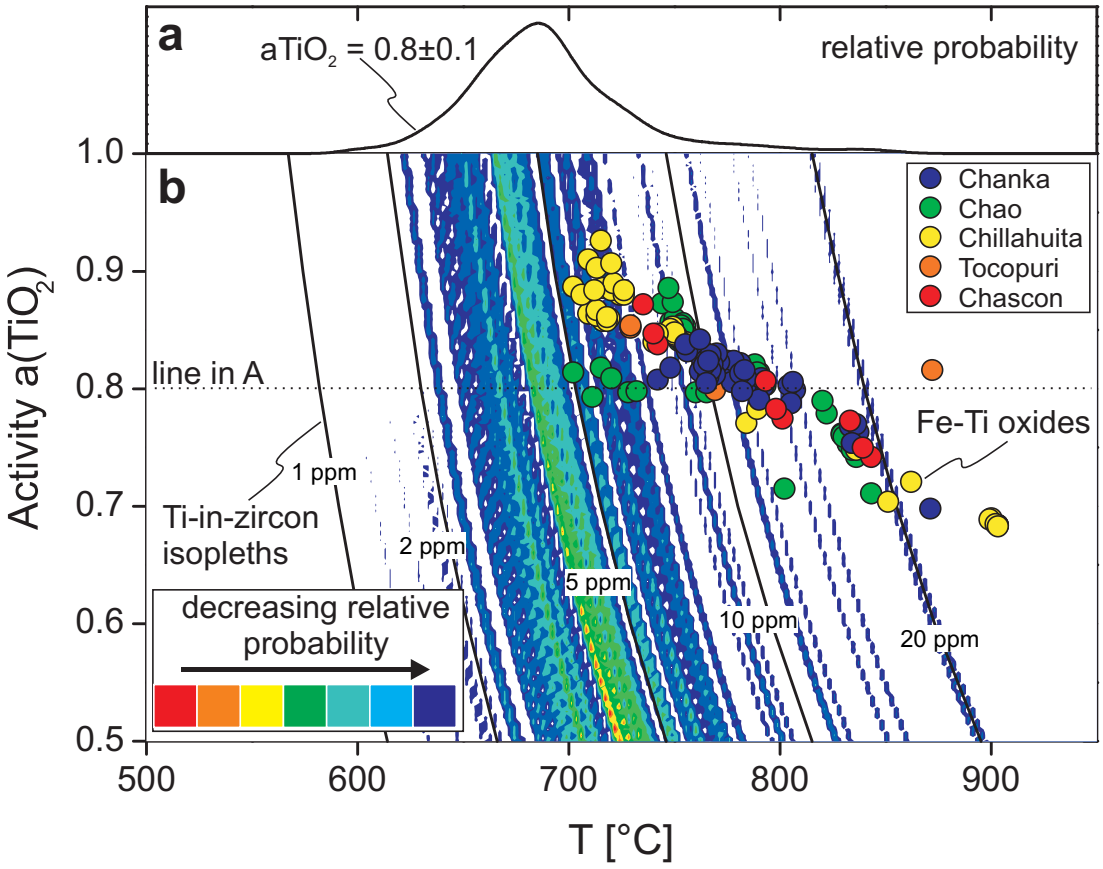

Tierney et al. Supplementary Figure 4

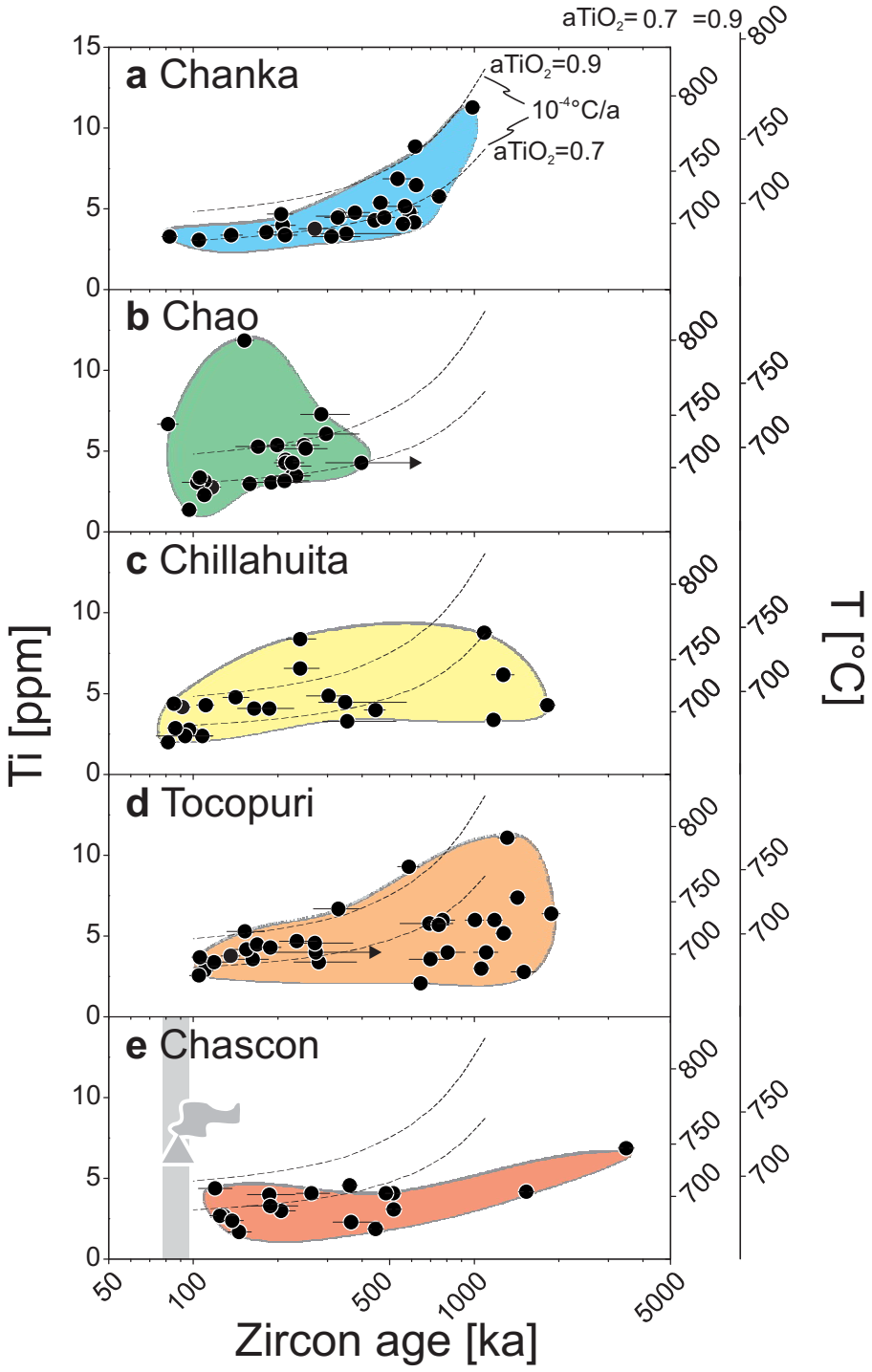

Tierney et al. Supplementary Figure 5

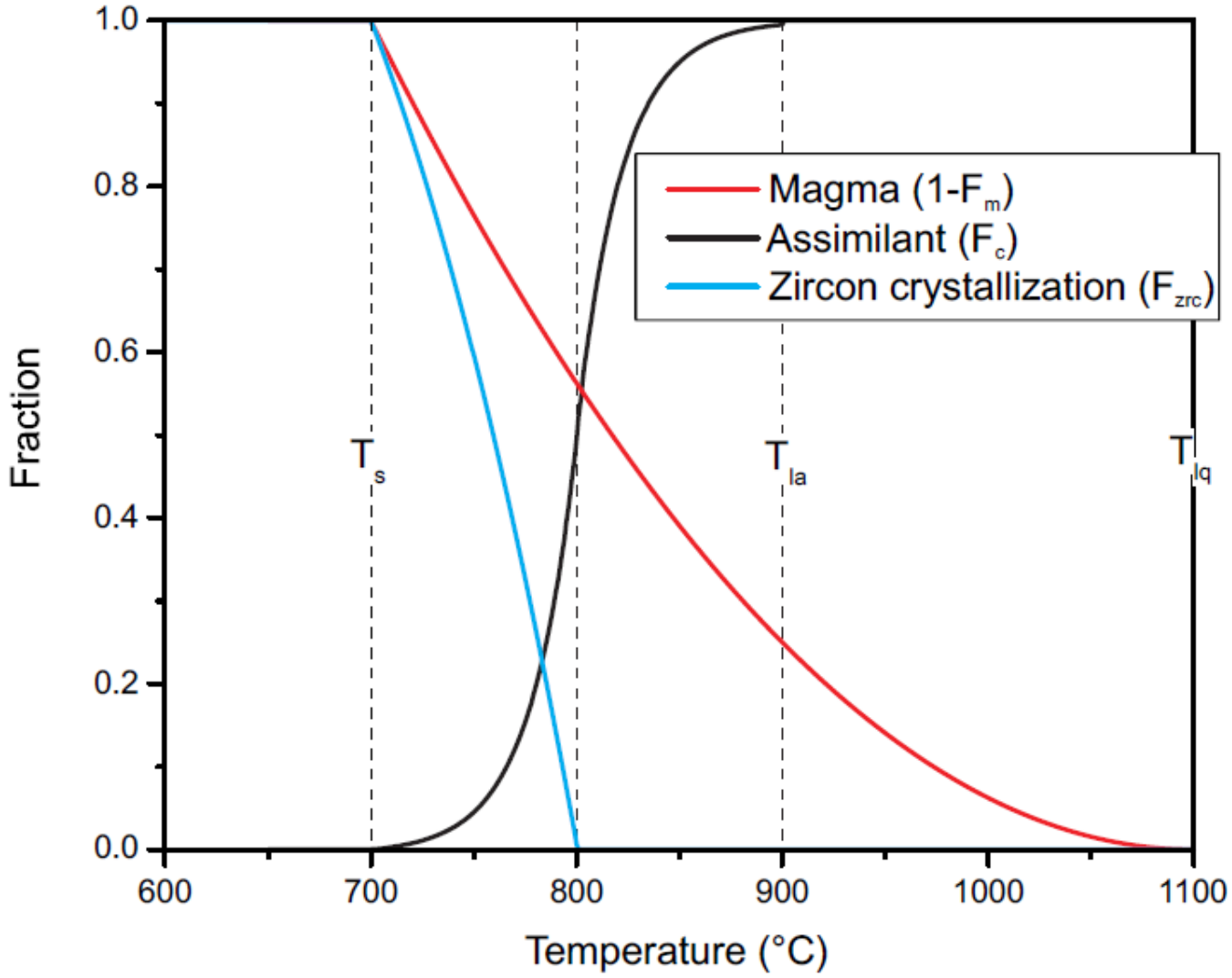

Tierney et al. Supplementary Figure 6

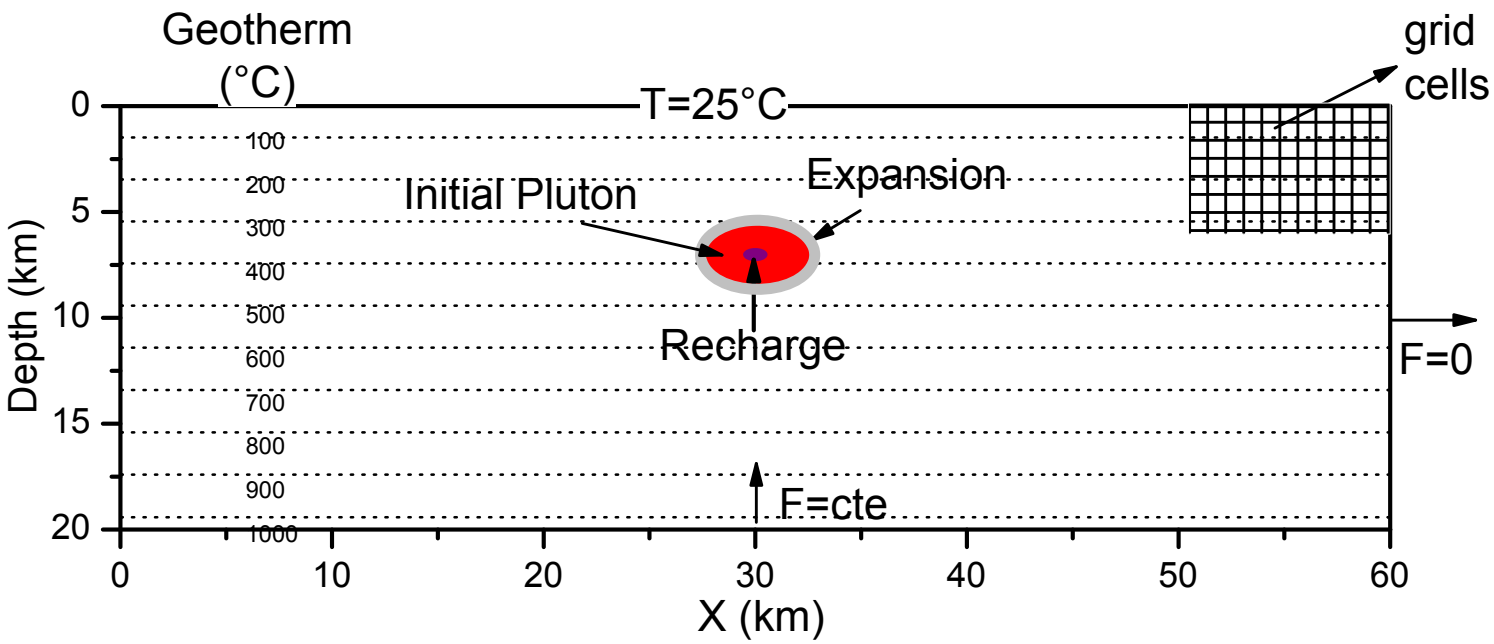

Tierney et al. Supplementary Figure 7

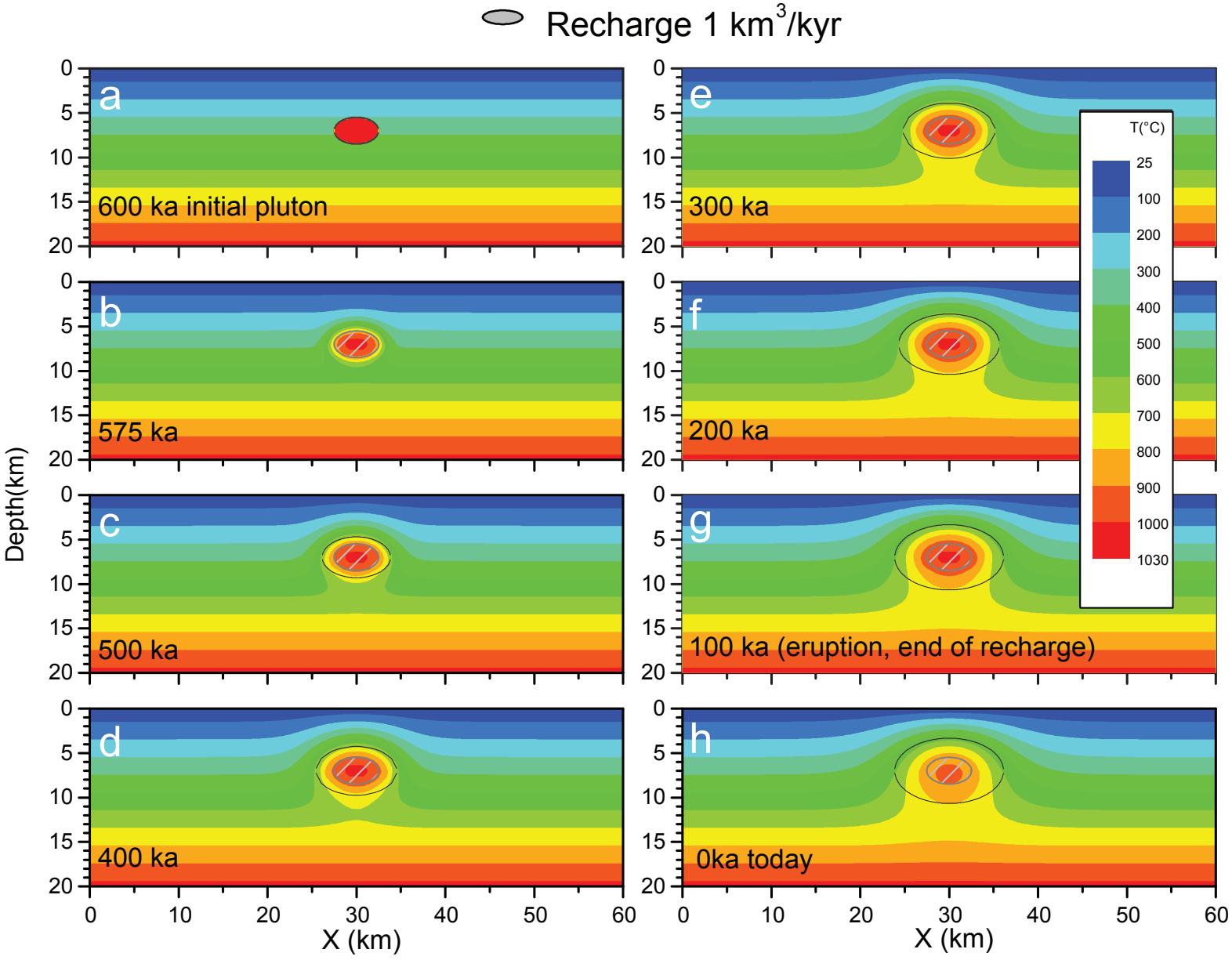

Tierney et al. Supplementary Figure 8

Table DR1

2016223 Table DR1 ArAr Ages FORMATTED.xlsx

Table DR2

2016223 Table DR2 Combined Zircon Data FORMATTED.xlsx

Table DR3. Thermal Model Parameters

Parameter	**Values**
Solidus Temperature	700 °C
Crust liquidus temperature	900 °C
Melt liquidus temperature	1100 °C
Specific fusion enthalpy	3.1 10^5 J/kg
Specific crystallization enthalpy	2.9 10^5 J/kg
Variable Thermal diffusivity and specific capacity	*See equation (1) in Supplementary Information*